High-Q Whispering-Gallery-Modes Microresonators for laser frequency locking in the Near-Ultraviolet Spectral Range

Georges Perin, Louis Ruel, Yannick Dumeige, Patrice Féron, Stephane Trebaol

High-Q Whispering-Gallery-Modes Microresonators for laser frequency locking in the Near-Ultraviolet Spectral Range

Georges Perin, Louis Ruel, Yannick Dumeige, Patrice Féron, and Stéphane Trebaol

***Abstract*—This study presents a comprehensive analysis of a whispering gallery mode (WGM) microsphere optical properties in the near ultraviolet spectrum, and its practical implementation for laser linewidth reduction via frequency locking. The light coupling is achieved thanks to the utilization of a robust angle-polished fiber, enabling exploration of various coupling behaviors. The intrinsic Q_0-factor, measured at 2.2×10^8, along with a finesse of 7.3×10^4, is reported at 420 nm. Physical mechanisms contributing to the Q_0-factor are discussed and routes to improve the performances are drawn. Through the implementation of frequency locking onto a high-Q resonance of the WGM microsphere, the reduction of the linewidth of an external cavity diode laser from 887 kHz to 91 kHz has been obtained. The study of these outcomes brings to performance assessment, enabling a thorough understanding of limitations and identifying potential pathways for enhancing noise reduction. Such high Q-factor and high finesse are key ingredients to ease the study of photonic devices based on WGM microresonators.**

***Index Terms*—Whispering gallery modes, microsphere, near ultraviolet, high Q-factor, frequency reference**

I. Introduction

WHISPERING gallery mode (WGM) microresonators have been extensively studied since decades for their unique properties like large Q-factor, long photon lifetime storage and small mode volume. Those unique features have allowed to demonstrate linear, non-linear and quantum photonic devices based on WGM resonators. Applications range from narrow-band filter [1], compact optical memory [2], optical [3] and electronic [4] locking for laser linewidth narrowing, Raman microlaser [5], on-chip frequency comb generation [6], low threshold lasing [7], biological sensing [8] or quantum electrodynamics experiments [9], [10]. Various shape of microresonators have been studied [8] such as microspheres, millidisks, microdisks and microtoroids in various materials like fused silica [11], fluoride and chalcogenide glasses or cristals [12]–[14]. Very high Q-factors have been reported up to 10^{10} in passive fused silica microspheres [15] and a record level of 3×10^{11} in CaF_2 crystalline millidisk resonators [16]. Despite the huge interest for those compact microresonators, they have been mainly studied in the near infrared region.

Since few years, the need of short wavelength compact coherent sources like single-frequency lasers and optical frequency combs, as tools for high precision spectroscopy [17], [18], pushes the research community to investigate the potential of WGM resonators at short wavelengths [12], [19]–[22]. In particular, millidisk configurations have been investigated with record Q-factors estimated to be as high as 10^9 at 370 nm [12]. Four wave mixing process have been recently demonstrated by Tian et al. [23] in a microsphere resonator at 460 nm with a 10^7 Q-factor. Moreover, microsphere resonator can be of interest in particular for QED experiment where high-Q factor should be associated with a small cavity volume [9].

In this work a thorough analysis of a fused silica WGM microsphere is reported at a wavelength of 420 nm. Subsequently, this microsphere serves as a frequency reference for the purpose of laser locking to demonstrate laser linewidth reduction. Thanks to the cavity ringdown method [24], we report an intrinsic microsphere Q-factor in excess to 10^8 limited by surface roughness. Robustness of the coupling setup based on angle-polished fiber offers the possibility to investigate the different coupling regimes. Critical coupling regime is obtained for a gap distance of 40 nm with a contrast of 100 %. In the near infrared region, water deposition on the microsphere surface degrades the Q-factor over time toward the 10^7 [15], [25]. Thanks to the water transparency window around 420 nm, no degradation is observed, which enables stable operation of WGM based photonic devices at short wavelengths. Then, the laser is locked to a high-Q WGM microsphere resonance, which allows the laser frequency noise to be reduced from 887 kHz to 91 kHz. This results points out the opportunity offered by such high-Q and high finesse compact optical resonators in the near UV range.

The paper is organised as follow, in section II, we report the fabrication process of the microspheres, in section III the coupling set-up based on an angle-polished fiber is described. Microsphere characterization is investigated in section IV, in particular, a description of the characterization technique that allows Q-factors and coupling regime determination is given. In section V, we discuss the mechanisms that contribute to the intrinsic Q-factor and identify the surface roughness as the main limitation. Lastly, in section VI, we outline the practical utilization of our microspheres, demonstrating a compact laser locking arrangement that enables the reduction of frequency noise of an external cavity diode laser in the near UV range.

II. Microsphere fabrication

Spherical microresonators are obtained by melting the tip of a pure silica fiber with a diameter of 125 μm (F300 from Heraeus). It turns that propagation losses in the fiber are given to be 30 dB/km around 420 nm. A fiber splicer is

Univ. Rennes, CNRS, Institut Foton - UMR 6082, F-22305 Lannion, France.
e-mail: stephane.trebaol@enssat.fr

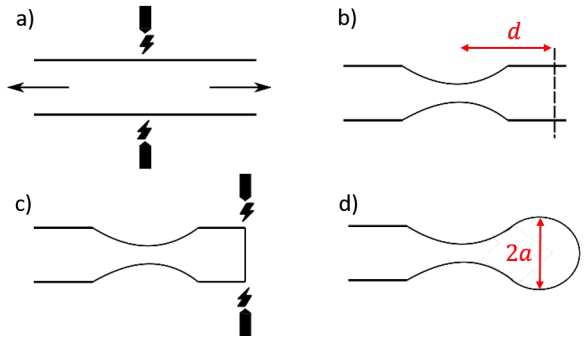

Fig. 1. Microspheres are fabricated in 3 steps by use of a fiber splicer. The heat source is brought by two electrodes placed on each side of the fiber. a) The fiber drawing gives rise to a fiber taper, b) the fiber is cleaved at a distance d from the taper region, to determine the quantity of silica to melt, c) the fiber tip is melted to form the microsphere, d) schematic of the final microsphere sample. a is the sphere radius.

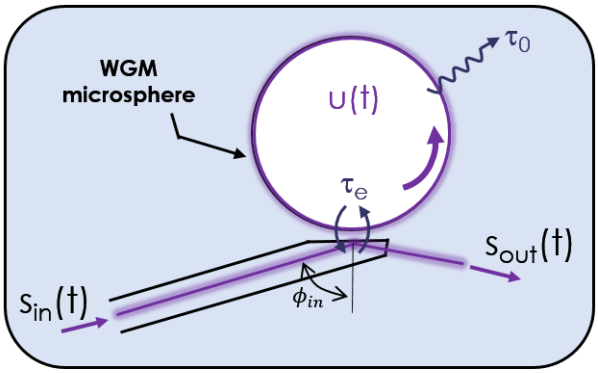

Fig. 2. Sketch of a WGM microsphere coupled to an angle-polished fiber pigtail. The input and output field are $s_{\text{in}}(t)$ and $s_{\text{out}}(t)$ respectively. $u(t)$ is the resonator mode amplitude, τ_0, the intrinsic photon lifetime and τ_e the coupling photon lifetime. ϕ_{in} stands for the optimal cutting angle used to reach the phase matching condition.

used to fabricate the microresonators. The three fabrication steps are shown on Figure 1. The heat source is brought by two electrodes that produce an electrical arc [26]. First, the fiber is elongated to form a taper with a central diameter below 50 μm and a narrowed region of around 700 μm in length. Then the fiber is cleaved at a distance d that sets the silica quantity brought for the sphere fabrication. The fiber diameter can be adjusted by varying d ($d \approx 1$ mm for a microsphere radius $a \approx 150$ μm) . Finally, the electrode driving current is appropriately adjusted to reach the glass transition temperature. The surface tension forces bring naturally a spheroid shape to the microresonator. Microsphere diameters ranging from 140 to 400 µm can be fabricated using this method. Inset of Figure 4 show a picture of the 275 μm diameter microsphere used in this work.

III. Angle-polished fiber coupling

Light in a WGM microresonator propagates along the surface by total internal reflection implying a strong light confinement and a high-Q factor. Reciprocally, the difficulty lies in an efficient light coupling inside the cavity. The solution consists in overlapping the WGM tail and the input beam evanescent field. To this end, three coupling systems are usually reported : prism [27], [28], tapered fiber [29] and angle-polished fiber [30]. In the present study, the angle-polished fiber have been implemented since it offers a good compromise in term of coupling efficiency, ease of implementation and robustness especially at short wavelengths where working distance between the microsphere and the coupling setup consists in few tens of nm. A schematic of the angle-polished fiber is shown on Figure 2. The light coupled inside the fiber core experiences a total internal reflection upon the angled surface. The evanescent part of the field is subsequently coupled into the microsphere. To obtain the phase matching between the waveguided mode and the considered microsphere WGM, one have to fulfill the following phase matching condition [30] :

$$\phi_{\text{in}} = \sin^{-1}\left(\frac{n_{\text{sphere}}}{n_{\text{fiber}}}\right) \tag{1}$$

where n_{sphere} is the effective refractive index of the WGM and n_{fiber} is the single-mode-fiber-effective refractive index. To determine the effective index for WGM modes inside the microsphere, we first have to calculate the resonant frequency of $\text{TE}_{l,m,q}$ using the following expressions [30], [31]:

$$\omega_{l,q} = \frac{c}{na}\left[\nu + 2^{-1/3}\alpha_q \nu^{1/3} - \frac{n}{\sqrt{n^2-1}}\right] \tag{2}$$

with l, m and q the polar, azimuthal and radial numbers of the electromagnetic field [11], c is the speed of light, n, the refractive index of silica ($n = 1.4681$ at 420 nm [32]), $\nu = l + \frac{1}{2}$, α_q is the q_{th} root of the Airy function $Ai(-z)$. The effective refractive index of the WGM is obtained from $n_{\text{sphere}} = cl/a\omega_{l,q}$. Figure 3 shows the value of n_{sphere} as a function of the microsphere radius for the fundamental and the two first high order WGMs ($q = 1, 2, 3$). For a microsphere diameter of 275 µm, the effective refractive index is $n_{\text{sphere}} = 1.4556(1.4460)$ for $q = 1(2)$.

The effective fiber index, n_{fiber} is experimentally determined to be 1.4675, which finally gives an angle-polished fiber $\phi_{\text{in}} = 82.7(80.2)°$ for $q = 1(2)$. We finally fabricate an angle-polished fiber with $\phi_{\text{in}} = 81 \pm 1°$ to couple light inside the microsphere. Considering TM modes for the angle-polished fiber design gives a similar value for ϕ_{in}.

To collect the signal extracted from the microsphere the tip of the fiber is cleaved perpendicularly to the light beam after reflection at the glass/air interface (see Figure 2). The gap between the fiber and the microsphere can be finely tune from 10 nm to few µm by step of 10 nm.

IV. Microsphere characterization

To characterize the microsphere and in particular to determine the quality factor of the resonator, usual laser scanning technique [33] cannot be used on high-Q ($Q > 10^7$) resonator. Indeed, thermal effects induced by material light absorption strongly distort the resonance [33] especially at short wavelengths where the linear absorption coefficient is 100 times larger than at telecom wavelengths. However, the cavity ringdown technique have been extensively used to determine the linear and nonlinear properties of high-Q

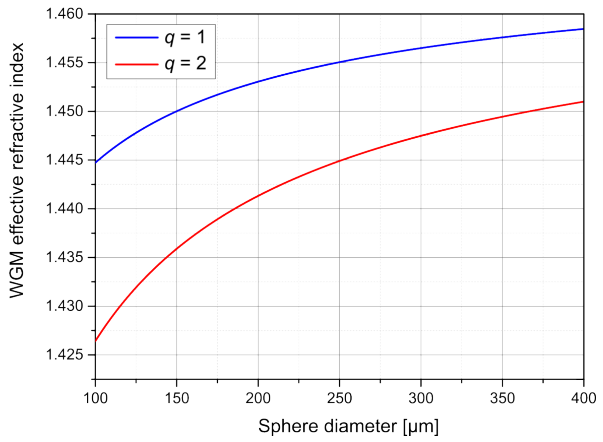

Fig. 3. Evolution of the effective refractive index n_{sphere} as a function of the microsphere radius a. The Airy function root values are 2.338 and 4.088 for $q = 1, 2$ respectively. The following parameter values are used: operating wavelength $\lambda = 420$ nm, silica optical index $n = 1.4681$, angular momentum l is obtained from $l = 2\pi an/\lambda$.

resonator [24], [34]–[36]. This technique allows to accurately estimate the intrinsic linear and nonlinear losses, the coupling regime and the linear and nonlinear dispersive properties of WGM resonators [37]. We propose in this paper to apply this technique to microspheres characterization close the near UV range at 420 nm.

A. System description

The fiber-coupled-microsphere experimental arrangement is depicted in Figure 2. The evanescent tail of the single-mode fiber is coupled into the probe WGM mode whose amplitude is $u(t)$. The coupling photon lifetime is expressed by τ_e and the intrinsic photon lifetime is denoted by τ_0. The later represents the microsphere losses experienced by the mode $u(t)$. The total lifetime is then deduced by $\tau^{-1} = \tau_0^{-1} + \tau_e^{-1}$ and the loaded Q-factor is expressed as $Q = \omega_0\tau/2$ where ω_0 is the angular frequency of the probed WGM. In the same way, the intrinsic Q-factor is given by $Q_0 = \omega_0\tau_0/2$.
For such high-finesse microresonator ($\mathcal{F} > 10^4$) the collected output signal $s_{\text{out}}(t)$ can be obtained from the input signal amplitude $s_{\text{in}}(t)$ by solving the following system [24]:

$$\begin{cases} \dfrac{du}{dt} = \left(\left[j\omega_0 - \frac{1}{\tau}\right]\right) u(t) + \sqrt{\frac{2}{\tau_e}} s_{\text{in}}(t) \\ s_{\text{out}}(t) = -s_{\text{in}} + \sqrt{\frac{2}{\tau_e}} u(t) \end{cases} \tag{3}$$

The instantaneous amplitude of the WGM $u(t)$ can be determine by integration of the system of equations (3). The amplitude $u(t)$ will strongly depends on the shape of the input signal $s_{\text{in}}(t)$. In this work we consider frequency chirped input signal which means that the carrier frequency is linearly swept in time such as $s_{\text{in}}(t) = s_0 e^{j\phi(t)}$ with $\phi(t) = \omega_i t + \pi V_S t^2$ where s_0 and ω_i are the amplitude and the initial angular frequency of the input signal respectively. V_S is the frequency scanning speed of the probe laser.

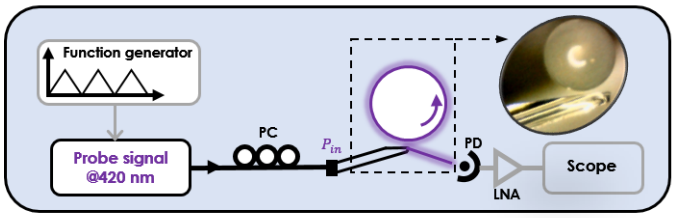

Fig. 4. Experimental setup for WGM microsphere characterization. PC, PD, and LNA stand for polarization controller, photodiode and low noise electrical amplifier respectively. P_{in} is the probe laser input power fixed at 4 mW. Inset: 275 μm diameter fiber coupled to a angle-polished fiber.

B. Cavity ringdown experimental setup

The experimental setup for the characterization of the resonators is presented in Figure 4. A single-mode laser source whose emission is centered around 420 nm and continuously tunable over 20 GHz is used to scan the resonances of the microresonator under test. The laser signal is injected, using the angle-polished fiber, in the resonator. The resonator is passively isolated on a stabilized table placed in a box in order to isolate it from environmental perturbations. The angle-polished fiber is inserted in a rotating stage allowing roll and pitch in addition to the *x, y, z* translations. At the output of the coupling fiber, light collection is carried out using a fast photodiode with a bandwidth of 2 GHz followed up by a low noise electrical amplifier wired to an oscilloscope.
The cavity ringdown technique consists in rapidly sweeping the frequency of the probe laser across a resonance of the cavity, i.e. faster than the relaxation time τ of the resonator, this leads to interference between the signal extracted from the cavity and the signal transmitted through the angle-polished fiber. The measured signal consists of oscillations with an exponentially decaying envelope as shown in Figure 5 a) (black curve).

C. Q-factors estimation

To estimate quality factors Q and Q_0 from the transmission signal, τ_0 and τ_e lifetimes are extracted by fitting the experimental curve with the theoretical model described above (see sec. IV-A). The fitting procedure is given in previous works [24], [36], [37]. The fitting parameters are the lifetimes τ_0 and τ_e, and the frequency scanning speed V_S. The fitting curve is displayed in red on Figure 5 a). A good overlap with the experimental curve is observed. Extracted parameters give $\tau_0 = 98 \pm 10$ ns, $\tau_e = 101 \pm 10$ ns, which gives a loaded Q-factor of $Q = (1.1 \pm 0.4) \times 10^8$ and an intrinsic Q- factor of $Q_0 = (2.2 \pm 0.4) \times 10^8$. Finally, thanks to the cavity ringdown measurement (CRDM) technique, linear parameters like τ_0 and τ_e can be evaluated. Then resonator transmission in the linear regime can be determined from [24]:

$$T(\delta) = \frac{(1/\tau_e - 1/\tau_0)^2 + 4\pi^2\delta^2}{(1/\tau_e + 1/\tau_0)^2 + 4\pi^2\delta^2} \tag{4}$$

with δ the frequency detuning from the resonance. The Lorentzian shape transmission spectrum is shown on Figure 5

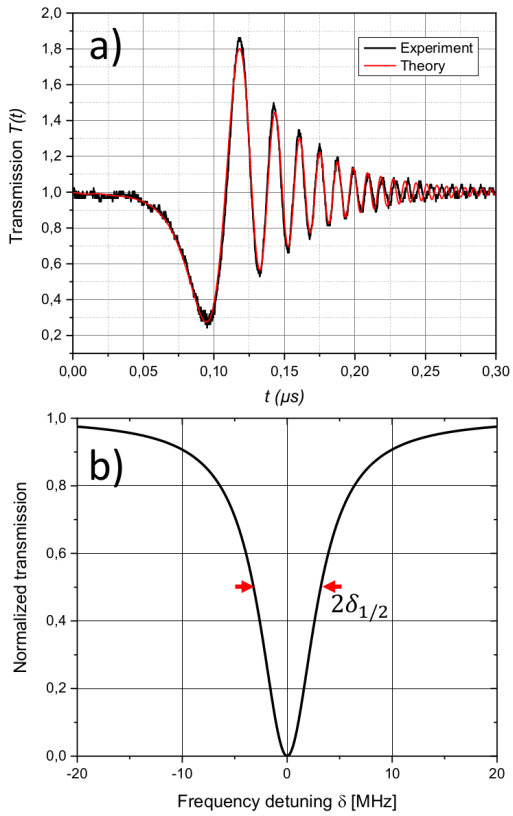

Fig. 5. a) Measured transmission (black curve) and fit (red curve) obtanined from a least sqaure method and the integration of Eqs. 3. This model give $\tau_0 = 98$ ns, $\tau_e = 101$ ns. b) Calculated Lorentzian shape transmission of the WGM microsphere from measured τ_0 and τ_e values using Eq.(4). The FWHM, $2\delta_{1/2}$, is evaluated to 6.5 MHz.

b). The full width at half-maximum (FWHM), $2\delta_{1/2}$ is related to the overall Q-factor by:

$$Q = \frac{\omega_0}{4\pi\delta_{1/2}} \tag{5}$$

which gives a FWHM, $2\delta_{1/2} = 6.5 \pm 2.4$ MHz.
It's noteworthy to mention that a detailed analysis of the alignment between the model and the experimental curve in Figure 5 a) reveals a minor discrepancy for the final oscillations (t > 0.2 μs). This slight shift arises from thermal effects, causing a resonance frequency drift as described in our previous paper [37]. In the present cavity ringdown characterization, the probe laser frequency is swept sufficently fast to minimize the contribution of the thermal effect. We verified that the use of a more detailed model including thermal effect (ref [37]) gives similar evaluation of τ_0 and τ_e.

D. Coupling regime versus coupling strength

The versatility of the angle-polished fiber allows the gap between the sphere and the coupling fiber to be finely tune by step of 10 nm. This offers the possibility to vary the coupling regime from undercoupling $\tau_e > \tau_0$ to overcoupling $\tau_e < \tau_0$ through the critical coupling regime $\tau_e = \tau_0$.
Figure 6 displays τ_0 and τ_e values for gap variations from 20 to 120 nm. First we can notice that $\tau_0 = 100 \pm 10$ ns is

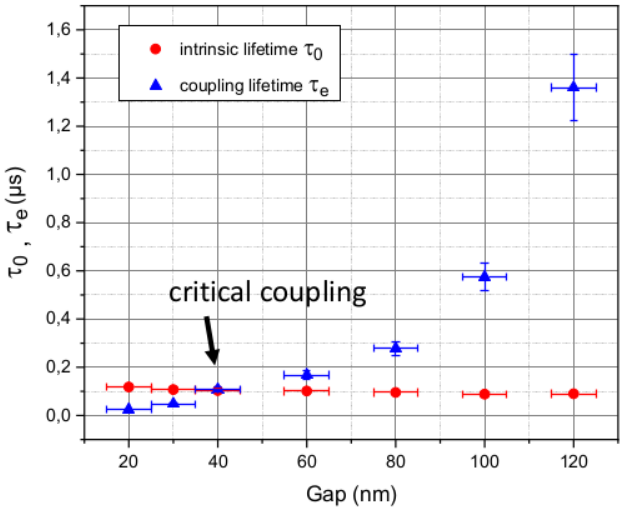

Fig. 6. Intrinsic and coupling lifetimes evolution versus the gap between the angle-polished fiber and the microsphere.

independent from gap variations. This was expected since the intrinsic photon lifetime refers to the optical losses inside the microsphere and then should not be affected by the coupling strength. The intrinsic Q-factor can then be estimated to be $(2.2 \pm 0.4) \times 10^8$ and the finesse to $\mathcal{F} = \lambda Q_0/(n\pi 2a) = (7.3 \pm 1.3) \times 10^4$. High finesse resonators highlight large intrinsic optical power. For example, an input power P_{in} = 1 mW gives an intrinsic optical power of $P \approx P_{\text{in}} 2\mathcal{F}/\pi \approx 46$ W. Resonators with high-Q and high finesse are good candidates to exhibit nonlinear effects.
The critical coupling regime is of interest for a large range of linear and nonlinear applications [23]. Here, our angle-polished fiber coupling set-up allows to obtain this regime with a contrast close to 100% for a gap value of 40 nm demonstrating the potential of this coupling tool for further investigations of microsphere-based photonic devices in the near-UV.

V. Limitation on the Q-factor in the near-UV

The light field propagating inside the cavity suffers from losses caused by various mechanisms [15]:

$$Q_0^{-1} = Q_{\text{rad}}^{-1} + Q_{\text{mat}}^{-1} + Q_{\text{surf}}^{-1} + Q_{\text{w}}^{-1} \tag{6}$$

Q_{rad} is related to the surface curvature, Q_{mat} to the material losses, Q_{surf} to the light scattering surface inhomogeneities and Q_{w} to absorption losses from water deposition on the microsphere surface. The radiative losses are usually very small [15] and do not contribute to the intrinsic Q-factor. When the condition $2a/\lambda \geq 15$ is reached, the Q_{rad} contribution to Q_0 is irrelevant, which is the case in the present study.
Light absorption in pure fused silica fiber is close to 30 dB/km at 420 nm [38], which gives :

$$Q_{\text{mat}} = \frac{2\pi n}{\alpha\lambda} \approx 3,1 \times 10^9 \tag{7}$$

As reported by Gorodestsky *et al.* [15], water absorption on the surface of the microsphere can contribute to the intrinsic Q-factor limitation [25]:

$$Q_{\mathrm{w}} \approx \sqrt{\frac{2a\pi}{8\lambda n^3}} \frac{1}{e\beta_w(\lambda)} \tag{8}$$

where e is the water layer thickness deposited on the microsphere surface and β_w the water absorption coefficient. For $e = 0.1$ nm [39] and $\beta_w = 0.00454$ m^{-1} at 420 nm [40], water absorption Q-factor is estimated to be $Q_w = 2 \times 10^{13}$ far above the measured Q_0 value. Here, we benefit from the water transparency window in the visible range. Contrary to reported studies in the NIR and (MIR) region, NUV fused silica microspheres do not suffer from water absorption that occurs minutes after the fabrication process.

The Q-factor related to surface scattering can be expressed as [41], [42]:

$$Q_{\mathrm{surf}} \approx \frac{3\lambda^3 a}{8n\pi^2 B^2 \sigma^2} \tag{9}$$

Inga *et al.* [26] evaluated, through AFM measurement, the rms roughness to be $\sigma = 0.4$ nm and a statistical correlation length $B = 90.6$ nm for fused silica microsphere fabricated using electric arc as it is done in the present paper. This gives a $Q_{\mathrm{surf}} = 2.0 \times 10^8$ at 420 nm, which is comparable to the measured intrinsic Q-factor. It is important to note that Q_{surf} (see Eq. (9)) is inversely proportional to the square of B and σ, and then strongly depends on this two parameters. Moreover, the method and the operation conditions for microsphere fabrication strongly affect measured values for B and σ [25], [43].

Figure 7 presents the contribution of the various Q-factors as a function of the wavelength for a given microsphere diameter of 275 µm. Physical limitations to the intrinsic Q-factor of fused silica microspheres strongly depend on the probing laser wavelength. Indeed, at telecom wavelengths the main limitation is related to water absorption at the surface of the sphere that degrades the Q-factor to the $10^7 - 10^8$ range after minutes. Then, specific microsphere packaging should be arranged to maintain a dry environment [15]. In the visible range, and in particular around 420 nm, water absorption is not an issue and the limiting effect is related to Rayleigh scattering due to surface inhomogeneities (see square box on Figure 7). Improvement in our microsphere fabrication process to reduce the surface imperfections should allow us to gain one order of magnitude on the Q_0 value.

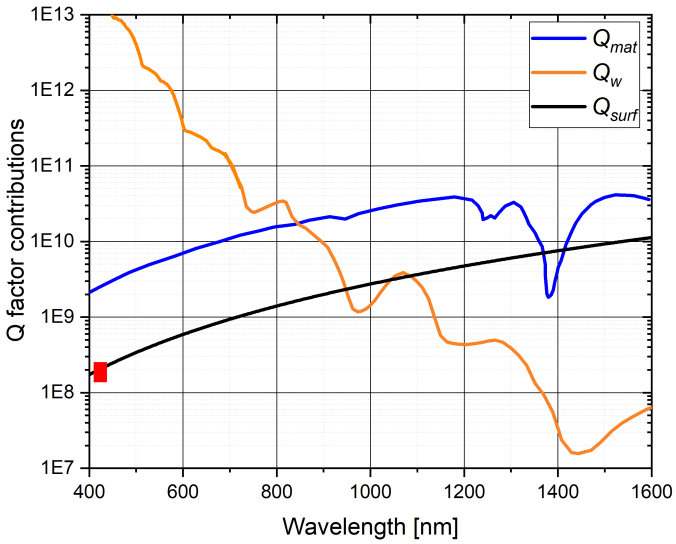

Fig. 7. Q-factor contributions to the intrinsic Q-factor. Q_{mat} is calculated from attenuation measurement on silica $F300$ by Humbach *et al.* [38]. Q_{w} is calculated from water absorption measurement from Pope *et al.* [40] for the visible range and from Palmer *et al.* [44] for the near infrared range. Red square correspond to the measured intrinsic Q-factor in this work.

VI. Application : Laser frequency locking

In this section we propose to study the potential of such high-Q and high finesse microspheres as frequency references in the near UV spectral range for laser stabilization. It has been already theoretically [45], [46] and experimentally [4], [47] demonstrated in the NIR range, that such WGM resonators can offer an interesting alternative to bulky frequency reference Fabry-Perot for applications where compactness is of concern. In the following, we report the linewidth narrowing of a 420 nm external-cavity diode laser (ECDL) by electronically locking the laser frequency to a high-Q WGM resonance by use of a Pound-Drever-Hall method.

A. Experimental set-up

The experimental scheme for the frequency locking is depicted in figure 8. For the locking, we introduce a modulation to the laser frequency by directly modulating the current controller using a locking amplifier set at 25 MHz. This modulation signal is then inserted in to the microsphere via the angle-polished fiber. The selected resonance for the reference has for parameters $\tau_0 = 100$ ns and $\tau_e = 1.3$ μs corresponding to a gap of 120 nm (cf. Fig. 6), which gives a quality factor of 7×10^7 and a contrast of 0.56. The optical signal at the output of the angle polished fiber is collected by a multimode fiber and sent to a photodetector. The photodetector output signal is then combined with the 25 MHz reference and subsequently filtered using the lock-in amplifier. The acquired error signal is send to the corrector, a proportional/integrate (PI) card, to generate a correction signal transmitted to the current controller for laser frequency stabilization.

In order to evaluate the effectiveness of the locking scheme, the frequency noise is characterized using a correlated delayed self-homodyne measurement setup, represented in the top part of figure 8. This setup consist of an unbalanced fiber-based Mach-Zehnder interferometer [48], enabling the characterization of the laser frequency noise power spectral density between DC and 1.3 MHz, with a noise floor level below 100 Hz^2/Hz in this configuration [49].

B. Results Analysis

We first measure the free-running frequency noise (FN) of the ECDL to evaluate subsequently the noise reduction once the laser is locked to a WGM resonance. The laser FN

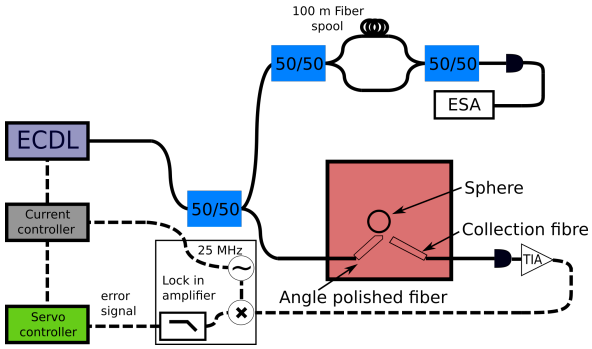

Fig. 8. Experimental setup for the locking of an ECDL on a 275 μm diameter passive microsphere. The servo controller is a PI card with a P value of 0.01 and I value of 4.7 MHz. These values have been selected to have a locking bandwith of 1MHz. The resonance used for the locking has a quality factor of 7×10^7 and a contrast of 0.56.

displays the usual behavior, exhibiting a slope of 1/f at low frequencies (below 100 kHz), followed by a characteristics white frequency noise at higher frequencies. This FN can be modeled by the expression $S_{\Delta\nu}(f) = h_{-1}/f + h_0$, with the free running laser parameters $h_{-1} = 144 \times 10^9$ Hz^3/Hz and $h_0 = 40 \times 10^3$ Hz^2/Hz are extracted experimentally. The intrinsic linewidth is then deduced from $\Delta\nu = \pi h_0$, which gives 126 kHz for the free running laser. The Elliott formula [50] enables to integrate the frequency noise, and thereby to deduce the integrated laser spectrum, as shown by the red curve in figure 9 b). From this curve, we estimate a linewidth of 887 kHz for an integration time of 10 ms.

The locked laser FN is also presented in Fig. 9 a) (green curve). From 100 Hz to 1 kHz, the FN exhibits few spikes, the overall level decreases to around 1×10^4 Hz^2/Hz, corresponding to a noise reduction of approximately 30 dB in comparison to the free-running laser at 1 kHz. For higher frequencies, the FN is maintained constant for a decade, and then gradually increases until it reaches the free-running FN at 500 kHz. The Elliott formula is used again to integrate the FN over the measurement bandwidth and to extract the locked laser spectrum, as depicted by the green curve in figure 9 b). Upon successful implementation of the locking scheme, a significant observation comes to light: the integrated linewidth undergoes a reduction from 887 to 91 kHz, representing a ratio of nearly 10. This promising outcome highlights the importance of delving into the various inherent limitations of this locking scheme.

The spikes centered around 250 Hz are attributed to lab devices acoustic and mechanical noises that perturb the sphere-to-fiber coupling distance. One way to mitigate this noise contribution is to fix the sphere and angle polished fiber on the same plate [51]. It is also important to enhance the isolation of the experiment by utilizing more elaborate active or passive noise reduction boxes [4].

In a previous study involving a fiber ring as a frequency reference, we developed a model to account for the various limitations induced by the experimental parameters and in particular those related to the frequency reference [49]. A derivation of this model is proposed in appendix for the case of a WGM microsphere. The result of the simulation is presented

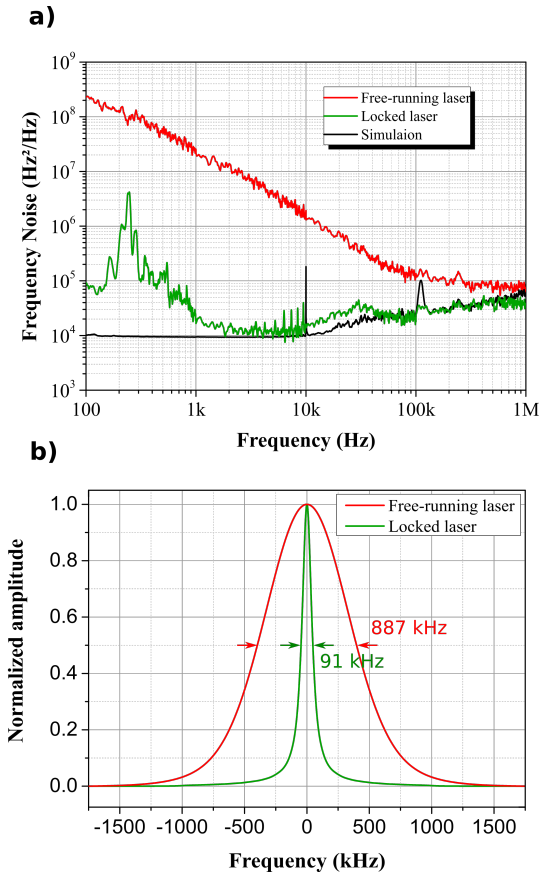

Fig. 9. a) Comparison between frequency noise of the free running laser (red curve), the locked laser (green curve), and the simulation with the discriminator noise contribution (black curve, Eq. 13). b) Comparison of the laser spectra extracted by the Elliott formula. The laser spectrum is shown in red for the free-running laser and in green for the locked laser.

in figure 9a) (black curve). It thus appears a good agreement between the measurement and the simulation, confirming that the noise floor observed beyond 1 kHz is attributable to a poor rejection of the photodetector shot noise. To improve the performance of the locking loop, it is then necessary to work with a WGM resonance with a more pronounced contrast and a higher quality factor, which would correspond to the operating point identified as "critical coupling" in figure 6. Nevertheless, such an operating point is accompanied by strong thermal non-linearities, which makes it difficult to lock the feedback loop. Due to locking instability, we have settled to use a gap distance of 120 nm. For smaller gaps, the locking was too unstable, while for larger gaps, the laser linewidth narrowing is degraded. The frequency drifts of WGM resonances induced by thermal effects have been intensively studied [52], [53] in the literature and solutions exist to overcome them. Thus, the deposition of coating having a negative thermal coefficient on the surface of the sphere can reduce or even eliminate the frequency drift [54], [55]. It should be noted that this is accompanied by a slight degradation of the quality factor. Furthermore, Grudinin et al. [56] proposed an experimental scheme involving a second laser to stabilize the frequency drifts. One can also investigate other materials with optical absorption coefficients lower than that of the pure silica used

in our study.

VII. Conclusion

We have presented a detailed characterization in the near UV of a WGM microsphere system in which light is coupled using an angle-polished fiber. Thanks to a cavity ringdown technique, intrinsic losses and coupling strength are deduced. An intrinsic Q_0-factor of 2.2×10^8 and a finesse of 7.3×10^4 are then reported. A revue on the physical mechanisms contributing to the intrinsic Q_0 factor is proposed. Contrary, to WGM microspheres probed in the near infrared region, surface-water-deposition-induced light absorption is not the limiting contribution thanks to the water transparency window around 420 nm. This independence to water absorption excludes the need to maintain a dry environment through appropriate packaging for further device integration. Scattering onto surface inhomogeneities have been identified as the limiting mechanism to the Q_0 factor in the 10^8 range. Improvement of the surface quality by optimizing the fabrication process should allow to gain one order of magnitude for the Q-factor. We also reported the implementation of the microsphere as a frequency reference for laser linewidth reduction. With a simple and compact optoelectronic locking scheme, we achieve a notable reduction of the laser locked frequency noise up to 30 dB within the 100 Hz-500 kHz range. This translates to a reduction of nearly a tenfold factor of the laser linewidth, shifting from 887 to 91 kHz. The experimental results are well reproduced by simulations pointing out that performances might be upgraded by using a higher Q-factor WGM resonance in critical coupling regime. The method of fabrication and characterization given in this paper might open the way towards photonic WGM microsphere based devices in the near-UV range.

Acknowledgment

The authors would like to thank Photonics Bretagne to provide the fiber sample for microsphere fabrication.
This work was supported by the Labex Cluster of Excellence FIRST-TF (ANR-10-LABX-48-01) within the Program "Investissements d'Avenir" and project COMBO (18-CE24-0003-01) both operated by the French National Research Agency (ANR).

APPENDIX

In order to determine the limitations of the frequency noise of the locked laser at frequencies higher than 1 kHz, we applied our previously developed model [49] to the case of the microsphere. The block diagram of the experimental setup is described in Fig. 10. The input variable of the servo loop is the central frequency ν_{ref} of the resonance. The output of the close loop ν_{lock} is compared to the reference frequency ν_{ref} to produce a frequency difference. The frequency difference is then converted into a voltage error signal ϵ through the frequency discriminator, represented by $K2$. The discriminator reflects the contribution of the resonance, the photodiode, the transimpedance gain, and the demodulation of the lock-in amplifier. The error signal ϵ is then converted into the correction signal S_{corr} through the PI corrector coefficients. Finally, the signal is converted into a frequency correction signal through the actuator $K1$, representing the current controller. Afterwards, the time-dependent frequency of the free-running laser $S_{\nu_{\text{ECDL}}}$ is added to the actuator output summing point. The laser's frequency is interpreted as a perturbation of the servo loop. Another perturbation is the shot noise generated by the photodetector N_{dis}, added to the output of the discriminator block.

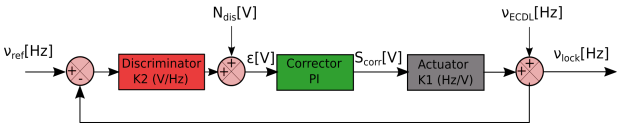

Fig. 10. Close loop block diagram of the ECDL locked on the sphere resonance (ν_{ref}). Various noise contributions are considered as the shot noise (N_{dis}) and the Free running laser noise (ν_{ECDL}). ν_{lock} corresponds to the FN of the locked laser

We can then express the open loop transfer function by:

$$G_{\text{OL}}(\omega) = K2C(\omega)K1(\omega) \tag{10}$$

with $C(\omega)$, the transfer function of the corrector, described by:

$$C(\omega) = g \times (P + \frac{1}{Ij\omega}) \tag{11}$$

Where g is the gain of the corrector, P and I are the proportional and integral parameters. Those values are chosen to reach a 1 MHz-correction bandwidth. Finally, the $K1$ coefficient (in Hz/V) describing the actuator is experimentally evaluated by using a swept sine method [57]. For the best locking result, the aim will be to maximise the open loop gain G_{OL}. Some limitation of the servo-loop can be highlighted by the close loop transfert function. It's important to note that we are working with random signals, thus we need to consider the power spectral density (expressed in Hz^2/Hz):

$$\begin{aligned} S_{\text{lock}} = \left|\frac{G_{\text{OL}}}{1+G_{\text{OL}}}\right|^2 S_{\nu_{\text{ref}}} + \\ \left|\frac{1}{1+G_{\text{OL}}}\right|^2 S_{\nu_{\text{ECDL}}} + \left|\frac{G_{\text{OL}}}{1+G_{\text{OL}}}\right|^2 \left|\frac{1}{K2}\right|^2 S_{N_{\text{dis}}} \end{aligned} \tag{12}$$

The frequency noise of the laser is composed of three noise contributions. The first one is associated with the noise of the reference. As we strive to maximize the open loop gain, the initial noise contribution is reduced to the noise of the reference, demonstrating that the locked laser noise can at best be equal to the noise of the reference. The second contribution depends on the free-running laser noise $S_{\nu_{\text{ECDL}}}$ and illustrates the effective noise reduction of the loop. The higher the open loop gain is, the lower this contribution will be. The last term is related to the shot noise and the discriminator $K2$. Similarly to the first term, as we increase the open loop gain, this term will be simplify to $S_Q = \left|\frac{1}{K2}\right|^2 S_{N_{\text{dis}}}$, which defines a limit.

This limit can be developed into the following expression (13) (the details that lead to this expression can be found in ref. [49]).

$$S_Q = \frac{q\Delta\nu^2}{16SPB^2}\left[\frac{1}{T_{max}J_1(\beta)^2} + \frac{2}{T_{min}J_0(\beta)^2}\right] \quad (13)$$

With T_{max} and T_{min} are the maximum and minimum resonance transmission, q the elementary electrical charge, Δ_ν the width of a resonance, S the photodiode responsivity, P the power at the input of the fiber ring, J_0 and J_1 the Bessel functions of the first kind, β the modulation index and $B = \frac{(1-\kappa)\sqrt{\kappa_c}}{\sqrt{\kappa}-\sqrt{\kappa_c}}$ a parameter depending of the transmission coefficient of the angle polished fiber κ and the round-trip losses $1-\kappa_c$. We can extract κ and κ_c from τ_e and τ_0, as described in [58]. With those values, we find $S_Q = 9200\ \mathrm{Hz}^2/\mathrm{Hz}$, and by plotting this limitation, we obtain the black curve on figure 9a), which shows that for frequencies above 1kHz, the limitation is indeed S_Q. This limitation expresses that for low frequency shifts of the laser, the gain of the discriminator K2 will not be significant enough to produce an error signal above the shot noise level of the photodetector.

REFERENCES

[1] M. C. Collodo, F. Sedlmeir, B. Sprenger, S. Svitlov, L. J. Wang, and H. G. L. Schwefel, "Sub-kHz lasing of a CaF_2 whispering gallery mode resonator stabilized fiber ring laser," *Optics Express*, vol. 22, p. 19277, Aug. 2014.

[2] V. Huet, A. Rasoloniaina, P. Guillemé, P. Rochard, P. Féron, M. Mortier, A. Levenson, K. Bencheikh, A. Yacomotti, and Y. Dumeige, "Millisecond Photon Lifetime in a Slow-Light Microcavity," *Physical Review Letters*, vol. 116, p. 133902, Mar. 2016.

[3] W. Liang, V. S. Ilchenko, D. Eliyahu, A. A. Savchenkov, A. B. Matsko, D. Seidel, and L. Maleki, "Ultralow noise miniature external cavity semiconductor laser," *Nature Communications*, vol. 6, p. 7371, Nov. 2015.

[4] J. Alnis, A. Schliesser, C. Wang, T. J. Kippenberg, and T. W. Hänsch, "Thermal-noise limited laser stabilization to a crystalline whispering-gallery mode resonator," in *CLEO/Europe and EQEC 2011 Conference Digest*, p. $EE2_6$, Optica Publishing Group, 2011.

[5] S. M. Spillane, T. J. Kippenberg, and K. J. Vahala, "Ultralow-threshold Raman laser using a spherical dielectric microcavity," *Nature*, vol. 415, pp. 621–623, Feb. 2002.

[6] P. Del'Haye, A. Schliesser, O. Arcizet, T. Wilken, R. Holzwarth, and T. J. Kippenberg, "Optical frequency comb generation from a monolithic microresonator," *Nature*, vol. 450, pp. 1214–1217, Dec. 2007.

[7] V. Sandoghdar, F. Treussart, J. Hare, V. Lefèvre-Seguin, J. M. Raimond, and S. Haroche, "Very low threshold whispering-gallery-mode microsphere laser," *Physical Review A*, vol. 54, pp. R1777–R1780, Sept. 1996.

[8] J. Ward and O. Benson, "WGM microresonators: sensing, lasing and fundamental optics with microspheres," *Laser Photonics Rev.*, no. 4, p. 18, 2011.

[9] J. R. Buck and H. J. Kimble, "Optimal sizes of dielectric microspheres for cavity QED with strong coupling," *Physical Review A*, vol. 67, p. 033806, Mar. 2003.

[10] C. Junge, D. O'Shea, J. Volz, and A. Rauschenbeutel, "Strong coupling between single atoms and non-transversal photons," *Physical Review Letters*, vol. 110, p. 213604, May 2013.

[11] A. Chiasera, Y. Dumeige, P. Féron, M. Ferrari, Y. Jestin, G. Nunzi Conti, S. Pelli, S. Soria, and G. Righini, "Spherical whispering-gallery-mode microresonators," *Laser & Photonics Reviews*, vol. 4, pp. 457–482, Apr. 2010.

[12] A. A. Savchenkov, S.-W. Chiow, M. Ghasemkhani, S. Williams, N. Yu, R. C. Stirbl, and A. B. Matsko, "Self-injection locking efficiency of a UV Fabry-Perot laser diode," *Optics Letters*, vol. 44, pp. 4175–4178, Sept. 2019.

[13] G. Lin, S. Diallo, K. Saleh, R. Martinenghi, J.-C. Beugnot, T. Sylvestre, and Y. K. Chembo, "Cascaded Brillouin lasing in monolithic barium fluoride whispering gallery mode resonators," *Applied Physics Letters*, vol. 105, p. 231103, Dec. 2014.

[14] G. R. Elliott, G. S. Murugan, J. S. Wilkinson, M. N. Zervas, and D. W. Hewak, "Chalcogenide glass microsphere laser," *Optics Express*, vol. 18, pp. 26720–26727, Dec. 2010.

[15] M. L. Gorodetsky, A. A. Savchenkov, and V. S. Ilchenko, "Ultimate Q of optical microsphere resonators," *Optics Letters*, vol. 21, pp. 453–455, Apr. 1996.

[16] A. A. Savchenkov, A. B. Matsko, V. S. Ilchenko, and L. Maleki, "Optical resonators with ten million finesse," *Optics Express*, vol. 15, pp. 6768–6773, May 2007.

[17] A. D. Ludlow, M. M. Boyd, J. Ye, E. Peik, and P. Schmidt, "Optical atomic clocks," *Reviews of Modern Physics*, vol. 87, pp. 637–701, June 2015.

[18] V. Maurice, V. Maurice, Z. L. Newman, Z. L. Newman, S. Dickerson, M. Rivers, J. Hsiao, P. Greene, M. Mescher, J. Kitching, M. T. Hummon, and C. Johnson, "Miniaturized optical frequency reference for next-generation portable optical clocks," *Optics Express*, vol. 28, pp. 24708–24720, Aug. 2020.

[19] P. S. Donvalkar, A. Savchenkov, and A. Matsko, "Self-injection locked blue laser," *Journal of Optics*, vol. 20, p. 045801, Feb. 2018.

[20] A. A. Savchenkov, J. E. Christensen, D. Hucul, W. C. Campbell, E. R. Hudson, S. Williams, and A. B. Matsko, "Application of a self-injection locked cyan laser for Barium ion cooling and spectroscopy," *Scientific Reports*, vol. 10, p. 16494, Oct. 2020.

[21] S. H. Lee, D. Y. Oh, Q.-F. Yang, B. Shen, H. Wang, K. Y. Yang, Y.-H. Lai, X. Yi, X. Li, and K. Vahala, "Towards visible soliton microcomb generation," *Nature Communications*, vol. 8, p. 1295, Nov. 2017.

[22] G. Lin, J. Fürst, D. V. Strekalov, I. S. Grudinin, and N. Yu, "High-Q UV whispering gallery mode resonators made of angle-cut BBO crystals," *Optics Express*, vol. 20, p. 21372, Sept. 2012.

[23] K. Tian, J. Yu, F. Lei, J. Ward, A. Li, P. Wang, and S. N. Chormaic, "Blue band nonlinear optics and photodarkening in silica microdevices," *Photon. Res.*, vol. 10, pp. 2073–2080, Sep 2022.

[24] Y. Dumeige, S. Trebaol, L. Ghişa, T. K. N. Nguyen, H. Tavernier, and P. Féron, "Determination of coupling regime of high-Q resonators and optical gain of highly selective amplifiers," *JOSA B*, vol. 25, no. 12, pp. 2073–2080, 2008.

[25] D. W. Vernooy, V. S. Ilchenko, H. Mabuchi, E. W. Streed, and H. J. Kimble, "High-Q measurements of fused-silica microspheres in the near infrared," *Optics Letters*, vol. 23, p. 247, Feb. 1998.

[26] M. Inga, L. Fujii, J. M. C. da Silva Filho, J. H. Quintino Palhares, A. S. Ferlauto, F. C. Marques, T. P. Mayer Alegre, and G. Wiederhecker, "Alumina coating for dispersion management in ultra-high Q microresonators," *APL Photonics*, vol. 5, p. 116107, Nov. 2020.

[27] V. Braginsky, M. Gorodetsky, and V. Ilchenko, "Quality-factor and nonlinear properties of optical whispering-gallery modes," *Physics Letters A*, vol. 137, pp. 393–397, May 1989.

[28] M. L. Gorodetsky and V. S. Ilchenko, "Optical microsphere resonators: optimal coupling to high-Q whispering gallery modes," *Journal of the Optical Society of America B*, vol. 16, p. 147, Jan. 1999.

[29] J. C. Knight, G. Cheung, F. Jacques, and T. A. Birks, "Phase-matched excitation of whispering-gallery-mode resonances by a fiber taper," *Optics Letters*, vol. 22, p. 1129, Aug. 1997.

[30] V. S. Ilchenko, X. S. Yao, and L. Maleki, "Pigtailing the high-Q microsphere cavity: a simple fiber coupler for optical whispering-gallery modes," *Optics Letters*, vol. 24, p. 723, June 1999.

[31] C. C. Lam, P. T. Leung, and K. Young, "Explicit asymptotic formulas for the positions, widths, and strengths of resonances in Mie scattering," *Journal of the Optical Society of America B*, vol. 9, p. 1585, Sept. 1992.

[32] I. H. Malitson, "Interspecimen Comparison of the Refractive Index of Fused Silica*,†," *JOSA*, vol. 55, pp. 1205–1209, Nov. 1965.

[33] T. Carmon, L. Yang, and K. J. Vahala, "Dynamical thermal behavior and thermal selfstability of microcavities," *Optics Express*, vol. 12, no. 20, pp. 4742–4750, 2004.

[34] G. N. Conti, S. Berneschi, F. Cosi, S. Pelli, S. Soria, G. C. Righini, M. Dispenza, and A. Secchi, "Planar coupling to high-q lithium niobate disk resonators," *Opt. Express*, vol. 19, pp. 3651–3656, Feb 2011.

[35] R. Henriet, G. Lin, A. Coillet, M. Jacquot, L. Furfaro, L. Larger, and Y. K. Chembo, "Kerr optical frequency comb generation in strontium fluoride whispering-gallery mode resonators with billion quality factor," *Optics letters*, vol. 40, pp. 1567–1570, Mar. 2015.

[36] A. Rasoloniaina, V. Huet, T. K. N. Nguyen, E. Le Cren, M. Mortier, L. Michely, Y. Dumeige, and P. Féron, "Controling the coupling properties of active ultrahigh-q wgm microcavities from undercoupling to selective amplification," *Scientific Reports*, vol. 4, p. 4023, 2014.

[37] A. Rasoloniaina, V. Huet, M. Thual, S. Balac, P. Féron, and Y. Dumeige, "Analysis of third-order nonlinearity effects in very high-q wgm res-

onator cavity ringdown spectroscopy," *JOSA B*, vol. 32, pp. 370–378, Feb. 2015.
[38] O. Humbach, H. Fabian, U. Grzesik, U. Haken, and W. Heitmann, "Analysis of OH absorption bands in synthetic silica," *Journal of Non-Crystalline Solids*, vol. 203, pp. 19–26, Aug. 1996.
[39] D. Ganta, E. Dale, and A. Rosenberger, "Measuring sub-nm adsorbed water layer thickness and desorption rate using a fused-silica whispering-gallery microresonator," *Measurement Science and Technology*, vol. 25, Apr. 2014.
[40] R. M. Pope and E. S. Fry, "Absorption spectrum (380–700 nm) of pure water II Integrating cavity measurements," *Applied Optics*, vol. 36, p. 8710, Nov. 1997.
[41] M. L. Gorodetsky, A. D. Pryamikov, and V. S. Ilchenko, "Rayleigh scattering in high-Q microspheres," *Journal of the Optical Society of America B*, vol. 17, p. 1051, June 2000.
[42] G. Lin, R. Henriet, A. Coillet, M. Jacquot, L. Furfaro, G. Cibiel, L. Larger, and Y. K. Chembo, "Dependence of quality factor on surface roughness in crystalline whispering-gallery mode resonators," *Optics Letters*, vol. 43, p. 495, Feb. 2018.
[43] X. Fan, *Cavity-QED studies of composite semiconductor nanostructure and dielectric microsphere systems*. PhD thesis, University of Oregon, 2000.
[44] K. F. Palmer and D. Williams, "Optical properties of water in the near infrared," *JOSA*, vol. 64, pp. 1107–1110, Aug. 1974.
[45] A. A. Savchenkov, A. B. Matsko, V. S. Ilchenko, N. Yu, and L. Maleki, "Whispering-gallery-mode resonators as frequency references II Stabilization," *Journal of the Optical Society of America B*, vol. 24, p. 2988, Dec. 2007.
[46] A. B. Matsko, A. A. Savchenkov, N. Yu, and L. Maleki, "Whispering-gallery-mode resonators as frequency references. i. fundamental limitations," *J. Opt. Soc. Am. B*, vol. 24, pp. 1324–1335, Jun 2007.
[47] T. Carmon, T. J. Kippenberg, L. Yang, H. Rokhsari, S. Spillane, and K. J. Vahala, "Feedback control of ultra-high-Q microcavities: application to micro-Raman lasers and micro-parametric oscillators," *Opt. Express*, vol. 13, pp. 3558–3566, May 2005.
[48] O. Llopis, P. H. Merrer, H. Brahimi, K. Saleh, and P. Lacroix, "Phase noise measurement of a narrow linewidth cw laser using delay line approaches.," *Optics letters*, vol. 36(14), pp. 2713–5, 2011.
[49] G. Perin, D. Mammez, A. Congar, P. Besnard, K. Manamanni, V. Roncin, F. D. Burck, and S. Trebaol, "Compact fiber-ring resonator for blue external cavity diode laser stabilization," *Optics Express*, vol. 29, pp. 37200–37210, Sep 2021.
[50] D. Elliott, R. Roy, and S. Smith, "Extracavity laser band-shape and bandwidth modification," *Physical Review A*, vol. 26, pp. 12–18, Jul 1982.
[51] Y. Dong, K. Wang, and X. Jin, "Packaged microsphere-taper coupling system with a high q factor," *Appl. Opt.*, vol. 54, pp. 277–284, Jan 2015.
[52] C. Schmidt, A. Chipouline, T. Pertsch, A. Tünnermann, O. Egorov, F. Lederer, and L. Deych, "Nonlinear thermal effects in optical microspheres at different wavelength sweeping speeds," *Opt. Express*, vol. 16, pp. 6285–6301, Apr 2008.
[53] X. Jiang and L. Yang, "Optothermal dynamics in whispering-gallery microresonators," *Light: Science & Applications*, vol. 9, p. 24, 02 2020.
[54] M. Han and A. Wang, "Temperature compensation of optical microresonators using a surface layer with negative thermo-optic coefficient," *Opt. Lett.*, vol. 32, pp. 1800–1802, Jul 2007.
[55] L. He, Y.-F. Xiao, C. Dong, J. Zhu, V. Gaddam, and L. Yang, "Compensation of thermal refraction effect in high-Q toroidal microresonator by polydimethylsiloxane coating," *Applied Physics Letters*, vol. 93, p. 201102, Nov. 2008.
[56] I. Grudinin, H. Lee, T. Chen, and K. Vahala, "Compensation of thermal nonlinearity effect in optical resonators," *Optics Express*, vol. 19, pp. 7365–7372, Apr. 2011.
[57] A. Novak, L. Simon, and P. Lotton, "Synchronized Swept-Sine: Theory, Application, and Implementation," *Journal of the Audio Engineering Society*, vol. 63, pp. 786–798, Nov. 2015.
[58] J.-B. Ceppe, *Eléments de dynamique du laser pour l'élaboration d'une source micro-onde miniaturisée sur la base de la double émission monomode d'un laser à mode de galerie*. Thèse, Université de Rennes 1 2018, 2018.